

Electronic Interactions and Thermal Disorder in Molecular Crystals Containing Cofacial Pentacene Units

Alessandro Troisi,^{*,†} Giorgio Orlandi,[†] and John E. Anthony[‡]

Dipartimento di Chimica 'G.Ciamician', Università di Bologna, via F. Selmi 2, 40126 Bologna, Italy, and Department of Chemistry, University of Kentucky, Lexington, Kentucky 40506

Received May 31, 2005. Revised Manuscript Received July 16, 2005

We computed the intermolecular electronic coupling and the band structure of three pentacene derivatives that stack cofacially in one or two dimensions. We rationalize the results building a map of the coupling between HOMOs and LUMOs of isolated pentacene molecules as a function of the relative molecular orientation and finding the position on such map of the actual molecular pairs. The apparently chaotic dependence of the intermolecular coupling from the crystal structure is explained, and directions for the design of materials with improved electric transport properties are given. We run molecular dynamics simulations to explore the variation of the intermolecular coupling due to the thermal motions. It is shown that, even in the crystal phase, the limited conformational space explored at room temperature is large enough to produce consistent variation in the intermolecular coupling. The consequences of this finding on the practicability of the transport properties of organic materials are analyzed.

1. Introduction

Synthetic chemistry and crystal engineering are providing a wide spectrum of solid compounds potentially useful as organic semiconductors,^{1–6} usually based on modified conjugated molecules such as polyacenes,^{7–10} polythiophenes,^{11–14} or hybrids thereof.^{15–18} The phenomenology of the measured charge transport properties in these materials is not completely understandable on the basis of the preexisting models employed for inorganic semiconductors, and a broad group

of theoretical physicists^{19–22} is trying to provide the appropriate framework for this problem. Computational chemistry and physics are acting, as usual, as a link between the experiment and the formal theory still under development.^{23–29}

If the transport can be described as bandlike, the coupling between molecular orbitals determines the band dispersion, the carrier effective mass, and—together with some additional information on the scattering rate—the charge carrier mobility. When the bandlike mechanism is active, the charge carriers are completely delocalized and the transport is described by the Boltzmann equation or other related formalisms. In the opposite limit of a purely hopping mechanism, the charge carriers are completely localized by the electron–phonon coupling (nuclear reorganization energy) and the hopping rate between neighboring sites is proportional to the square of the electronic coupling between localized wave functions. Although the actual transport mechanism is probably intermediate between the two regimes, in both cases the best transport properties are obtained for materials that display the larger possible electronic coupling between neighboring molecules. The challenge of crystal engineering applied to organic semiconductor is to

* Corresponding author. E-mail: alessandro.troisi@unibo.it.

[†] Università di Bologna.

[‡] University of Kentucky.

- (1) Dimitrakopoulos, C. D.; Malenfant, P. R. L. *Adv. Mater.* **2002**, *14*, 99.
- (2) Horowitz, G. *J. Mater. Res.* **2004**, *19*, 1946.
- (3) Witte, G.; Woell, C. *J. Mater. Res.* **2004**, *19*, 1889.
- (4) Katz, H. E. *Chem. Mater.* **2004**, *16*, 4748.
- (5) Newman, C. R.; Frisbie, C. D.; da Silva, D. A.; Brédas, J. L.; Ewbank, P. C.; Mann, K. R. *Chem. Mater.* **2004**, *16*, 4436.
- (6) Bendikov, M.; Wudl, F.; Perepichka, D. F. *Chem. Rev.* **2004**, *104*, 4891.
- (7) Anthony, J. E.; Brooks, J. S.; Eaton, D. L.; Parkin, S. R. *J. Am. Chem. Soc.* **2001**, *123*, 9482.
- (8) Ito, K.; Suzuki, T.; Sakamoto, Y.; Kubota, D.; Inoue, Y.; Sato, F.; Tokito, S. *Angew. Chem., Int. Ed.* **2003**, *42*, 1159.
- (9) Moon, H.; Zeis, R.; Borkent, E. J.; Besnard, C.; Lovinger, A. J.; Siegrist, T.; Kloc, C.; Bao, Z. N. *J. Am. Chem. Soc.* **2004**, *126*, 15322.
- (10) Sundar, V. C.; Zaumseil, J.; Podzorov, V.; Menard, E.; Willett, R. L.; Someya, T.; Gershenson, M. E.; Rogers, J. A. *Science* **2004**, *303*, 1644.
- (11) Katz, H. E.; Lovinger, A. J.; Laquindanum, J. G. *Chem. Mater.* **1998**, *10*, 457.
- (12) Granstrom, E. L.; Frisbie, C. D. *J. Phys. Chem. B* **1999**, *103*, 8842.
- (13) Facchetti, A.; Mushrush, M.; Yoon, M. H.; Hutchison, G. R.; Ratner, M. A.; Marks, T. J. *J. Am. Chem. Soc.* **2004**, *126*, 13859.
- (14) Facchetti, A.; Yoon, M.-H.; Stern, C. L.; Katz, H. E.; Marks, T. J. *Angew. Chem., Int. Ed.* **2003**, *42*, 3900.
- (15) Laquindanum, J. G.; Katz, H. E.; Lovinger, A. J. *J. Am. Chem. Soc.* **1998**, *120*, 664.
- (16) Facchetti, A.; Letizia, J.; Yoon, M. H.; Mushrush, M.; Katz, H. E.; Marks, T. J. *Chem. Mater.* **2004**, *16*, 4715.
- (17) Meng, H.; Sun, F. P.; Goldfinger, M. B.; Jaycox, G. D.; Li, Z. G.; Marshall, W. J.; Blackman, G. S. *J. Am. Chem. Soc.* **2005**, *127*, 2406.
- (18) Merlo, J. A.; Newman, C. R.; Gerlach, C. P.; Kelley, T. W.; Muires, D. V.; Fritz, S. E.; Toney, M. F.; Frisbie, C. D. *J. Am. Chem. Soc.* **2005**, *127*, 3997.

- (19) Kenkre, V. M. *Phys. Lett. A* **2002**, *305*, 443.
- (20) Giuggioli, L.; Andersen, J. D.; Kenkre, V. M. *Phys. Rev. B* **2003**, *67*, 045110.
- (21) Fratini, S.; Ciuchi, S. *Phys. Rev. Lett.* **2003**, *91*, 256403.
- (22) Hannewald, K.; Stojanovic, V. M.; Schellekens, J. M. T.; Bobbert, P. A.; Kresse, G.; Hafner, J. *Phys. Rev. B* **2004**, *69*, 075211.
- (23) Cheng, Y. C.; Silbey, R. J.; da Silva Filho, D. A.; Calbert, J. P.; Cornil, J.; Brédas, J. L. *J. Chem. Phys.* **2003**, *118*, 3764.
- (24) Hutchison, G. R.; Ratner, M. A.; Marks, T. J. *J. Phys. Chem. A* **2002**, *106*, 10596.
- (25) de Wijs, G. A.; Mattheus, C. C.; de Groot, R. A.; Palstra, T. T. M. *Synth. Met.* **2003**, *139*, 109.
- (26) Brédas, J. L.; Beljonne, D.; Coropceanu, V.; Cornil, J. *Chem. Rev.* **2004**, *104*, 4971.
- (27) Troisi, A.; Orlandi, G. *J. Phys. Chem. B* **2005**, *109*, 1849.
- (28) Huang, J.; Kertesz, M. *Chem. Phys. Lett.* **2004**, *390*, 110.
- (29) Hutchison, G. R.; Ratner, M. A.; Marks, T. J. *J. Am. Chem. Soc.* **2005**, *127*, 2339.

design systems with the maximum electronic interaction between its molecular components.

Most of the conjugated molecule/polymer proposed for organic electronics stacks in herringbone fashion (unsubstituted pentacene, thiophene, polyphenylene). π -Stacking among cofacial molecules is rarer: it is displayed, for example, by discotic material,^{30,31} DNA base pairs,^{32,33} poly-(3-alkylthiophene),³⁴ and dithiophene-tetrathiafulvalene.³⁵ A wide set of solids displaying cofacial packing among its conjugated components was prepared by Anthony and co-workers,^{7,36} who synthesized materials based on pentacene with bulky substituents in positions 6,13 or 5,14.

These materials, substituted with trialkylsilyl groups, are highly soluble, very stable, and form large crystals easily by solution crystallization methods. The nature and amount of π -overlap in these materials is controlled by altering the size or location of the functional group.³⁶ Although a number of derivatives have been reported, all of the stacking motifs fall into three general categories (see Figure 1): *1-D slipped-stack* (exemplified by TMS, i.e., 6,13-bis(trimethylsilylethynyl)pentacene), *columnar π -stack* (exemplified by TESO, i.e., 5,14-bis(triethylsilylethynyl)pentacene, with substituents offset with respect to the center), and *2-D π -stacking* (exemplified by TIPS, i.e., 6,13-bis(triisopropylsilylethynyl)pentacene). Of all the functionalized pentacene molecules tested, only the 2-D π -stacking materials exhibit significant hole mobilities (up to 0.4 cm²/V s for TIPS).³⁷ Because of the ease with which crystal packing in this class of materials can be “fine-tuned”, working models that give direction to the crystal engineering process will greatly accelerate the development and utilization of useful materials.

In this paper, we compute the intermolecular electronic coupling between neighboring molecules of the ordered crystals of TMS, TIPS and TESO and their band structure. After describing the method and illustrating the results (section 2), we suggest a rationalization, identifying some common characteristics in the intermolecular coupling for material based on coplanar conjugated carbon molecules (section 3). We will show in section 4 how the thermal motions can dramatically affect the transport properties of this class of materials. In the conclusion, we discuss how the findings of this paper might affect the strategies for the design of better organic semiconductors.

2. Electronic Structure of the Three Solids

Method. To compute the band structure of the three solids, we used a slightly modified version of a method described

- (30) vandeCraats, A. M.; Warman, J. M.; deHaas, M. P.; Adam, D.; Simmerer, J.; Haarer, D.; Schuhmacher, P. *Adv. Mater.* **1996**, *8*, 823.
 (31) Wu, J. H.; Watson, M. D.; Mullen, K. *Angew. Chem., Int. Ed.* **2003**, *42*, 5329.
 (32) Giese, B.; Wessely, S.; Spormann, M.; Lindemann, U.; Meggers, E.; Michel-Beyerle, M. E. *Angew. Chem. Int. Ed.* **1999**, *38*, 996.
 (33) O'Neill, M. A.; Barton, J. K. *J. Am. Chem. Soc.* **2004**, *126*, 11471.
 (34) Sirringhaus, H.; Brown, P. J.; Friend, R. H.; Nielsen, M. M.; Bechgaard, K.; Langeveld-Voss, B. M. W.; Spiering, A. J. H.; Janssen, R. A. J.; Meijer, E. W.; Herwig, P.; de Leeuw, D. M. *Nature* **1999**, *401*, 685.
 (35) Mas-Torrent, M.; Durkut, M.; Hadley, P.; Ribas, X.; Rovira, C. *J. Am. Chem. Soc.* **2004**, *126*, 984.
 (36) Anthony, J. E.; Eaton, D. L.; Parkin, S. R. *Org. Lett.* **2002**, *4*, 15.
 (37) Sheraw, C. D.; Jackson, T. N.; Eaton, D. L.; Anthony, J. E. *Adv. Mater.* **2003**, *15*, 2009.

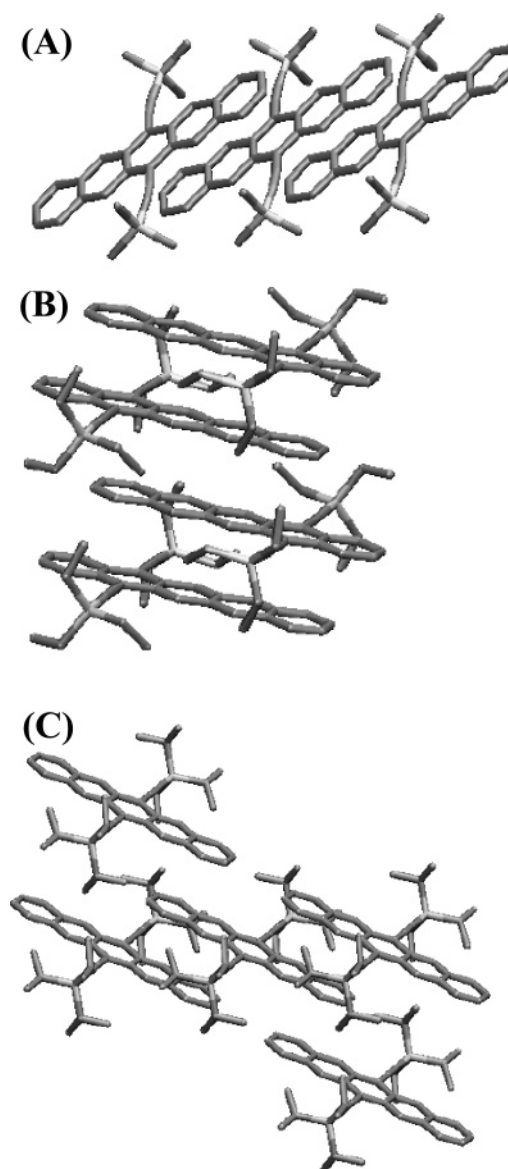


Figure 1. Packing motifs of the three systems studied in this paper (A) slip stacks of TMS, (B) columnar stacks of TESO, and (C) segregated stacks of TIPS.

in detail in ref 27, which we briefly recall. This method is akin to the approach often referred as the “dimer method”.²⁶ We first compute, for all the molecules in the unit cell, the molecular orbitals (MO) of the isolated molecule (we will refer to them as *unperturbed* MOs). We consider only a subset of MOs, usually four frontier orbitals, i.e., the two highest energy occupied and the two lowest energy unoccupied orbitals per molecule. This set, $\{\phi_\alpha\}$, can be used to form the Bloch-type basis functions for the calculation of the band structure. We compute the interorbital coupling V between neighboring molecules and their overlap S as:

$$V_{\alpha\beta T} = \langle \phi_\alpha(r) | H^{\text{eff}} | \phi_\beta(r - T) \rangle \quad (1)$$

$$S_{\alpha\beta T} = \langle \phi_\alpha(r) | \phi_\beta(r - T) \rangle \quad (2)$$

H^{eff} is an effective one-electron Hamiltonian, usually of the same type used to compute the unperturbed orbitals. T is an element of the direct lattice with unit vectors \vec{a} , \vec{b} , and \vec{c} ($T = n_a\vec{a} + n_b\vec{b} + n_c\vec{c}$, with n_a , n_b , and n_c integer numbers).

The matrix elements in eqs 1 and 2 involve the orbital ϕ_α and the orbital ϕ_β , the latter translated by a lattice vector T . Identifying with k a vector in the reciprocal space ($k = x_a\vec{a}^* + x_b\vec{b}^* + x_c\vec{c}^*$, with x_a , x_b , and x_c real), the band energies ϵ^k for each k value are a solution of the generalized eigenvalues equation:

$$\mathbf{H}^k \mathbf{C}^k = \mathbf{S}^k \mathbf{C}^k \epsilon^k \quad (3)$$

with the matrixes \mathbf{H}^k and \mathbf{S}^k given by

$$H_{\alpha\beta}^k = \sum_T V_{\alpha\beta T} \exp(ikT) \quad (4)$$

$$S_{\alpha\beta}^k = \sum_T S_{\alpha\beta T} \exp(ikT) \quad (5)$$

We computed the orbitals of the isolated molecules $\{\phi_\alpha\}$ at the B3LYP level with the 6-31G* basis set. H^{eff} in eq 1 could be therefore chosen simply as the (B3LYP) Fock–Kohn–Sham operator³⁸ for the couple of molecules implied by eq 1. This was the choice made in ref 27 and it is sufficiently accurate when there is nonnegligible overlap between the frontier orbitals of neighboring molecules. In this case, however, there are couples of molecules that are in contact through their alkylic portion, i.e., the interaction between the frontier orbitals (localized on the pentacene units) can be also mediated by orbitals localized on the saturated fragment. The situation is analogous to that of donor–bridge–acceptor molecules in which the donor–acceptor interaction is mediated by a saturated bridge.^{39,40} One trivial way to study this case requires the inclusion of all the MOs on each molecule in the calculation of the band, but this approach could complicate the analysis of the results. Instead, we use the matrix partition method^{40,41} to compute from the total one-electron Hamiltonian of a couple of molecules a *reduced Hamiltonian* that includes only the frontier orbital but accounts effectively for the presence of other orbitals that could mediate the intermolecular coupling. The implications of this method have been widely discussed in the charge-transfer literature,^{42,43} and we simply use the main result.

The full orbital space is divided into two subspaces: the F subspace, containing only the frontier orbitals, and the G subspace, containing all the other orbitals. The total Hamiltonian of the couple of molecules (and similarly the overlap matrix \mathbf{S}) is partitioned as

$$\mathbf{H} = \begin{bmatrix} \mathbf{H}_{FF} & \mathbf{H}_{FG} \\ \mathbf{H}_{GF} & \mathbf{H}_{GG} \end{bmatrix} \quad (6)$$

The effective Hamiltonian in the subspace of the frontiers orbital is

$$\mathbf{H}_{FF}^{\text{eff}}(E) = \mathbf{H}_{FF} + (\mathbf{H}_{FG} - E\mathbf{S}_{FG})(E\mathbf{S}_{GG} - \mathbf{H}_{GG})^{-1}(\mathbf{H}_{GF} - E\mathbf{S}_{GF}) \quad (7)$$

The first term in the right-hand side of eq 7 corresponds to the direct coupling between the frontier orbitals, and the second term is the correction due to the coupling through orbitals external to the frontier orbital subspace. The

Table 1. Selected Electronic Couplings between MOs Localized on Close Molecules for the Three Considered Molecular Solids^a

TMS	m	n_a	n_b	n_c	$V_{\text{HH}}(\text{cm}^{-1})$	$V_{\text{LL}}(\text{cm}^{-1})$
a	1	0	0	1	2.7	2.1
	1	0	1	0	22.5	0.7
	1	0	1	1	12.2	-13.4
	1	1	-1	-1	-0.2	0.2
	1	1	-1	0	54.5	58.1
	1	1	0	0	358.0	1839.6
	1	1	0	1	-4.3	-2.4
	1	1	1	1	-0.4	0.7
TESo	m	n_a	n_b	n_c	H–H	L–L
b	1	0	1	0	-6.2	-0.9
	2	-1	0	0	14.2	-8.0
	2	0	-1	0	14.2	-8.0
	3	0	-1	0	-0.4	0.7
	3	0	0	0	-0.4	0.7
	4	-1	0	-1	0.0	0.0
	4	0	-1	0	8.3	-10.3
	4	0	0	0	67.1	-26.3
	4	0	1	0	8.3	-10.3
	5	0	-1	0	76.9	3.5
	5	0	0	0	9.4	-1.5
	6	0	0	0	136.7	-1129.2
	6	0	1	0	-472.2	804.0
	7	-1	0	-1	0.5	0.2
	7	-1	1	-1	1.8	-0.1
	7	0	0	0	0.5	0.2
7	0	1	0	1.8	-0.1	
8	0	-1	-1	3.7	4.8	
8	0	-1	0	3.7	4.8	
8	0	0	-1	0.9	1.6	
8	0	0	0	0.9	1.6	
TIPS	m	n_a	n_b	n_c	H–H	L–L
d	1	0	0	1	-1.6	0.5
	1	0	1	-1	-1.8	2.1
	1	0	1	0	-14.8	-2.9
	1	1	-1	0	34.3	652.7
	1	1	0	-1	0.2	0.1
	1	1	0	0	237.8	-1514.1
e	1	1	1	-1	0.7	-1.0

^a We included only the coupling between HOMOs (V_{HH}) and LUMOs (V_{LL}). Each row reports the coupling between the first and the m th molecule of the unit cell,²⁷ with the m th molecule translated by $T = n_a\vec{a} + n_b\vec{b} + n_c\vec{c}$. The labels **a–e** indicate the most strongly interacting couples discussed in the text.

parameter E is conveniently set to the average energy of the unperturbed frontier orbitals.⁴⁰

The computational procedure can be summarized as follows: (i) a list of couples of interacting molecules is compiled;⁴⁴ (ii) For each couple the \mathbf{H} and \mathbf{S} matrixes in the basis of the unperturbed MO are computed; (iii) the effective coupling between the frontier orbitals is computed using eq 7 and will form the set of matrix elements $\{V_{\alpha\beta T}\}$; (iv) the global Hamiltonian of the solid is built using eq 1, and the band dispersion is computed from eq 3.

The computation is performed on the geometries obtained by X-ray crystallography and published in refs 36 and 7.

(38) Parr, G. R.; Yang, W. *Density-Functional Theory of Atoms and Molecules*; Oxford University Press: New York, 1994.

(39) Ratner, M. A. *J. Phys. Chem.* **1990**, *94*, 4877.

(40) Skourtis, S. S.; Beratan, D. N. *Adv. Chem. Phys.* **1999**, *106*, 377.

(41) Priyadarshy, S.; Skourtis, S. S.; Risser, S. M.; Beratan, D. N. *J. Chem. Phys.* **1996**, *104*, 9473.

(42) Troisi, A.; Ratner, M. A.; Zimmt, M. B. *J. Am. Chem. Soc.* **2004**, *126*, 2215.

(43) Troisi, A.; Orlandi, G. *J. Phys. Chem. B* **2002**, *106*, 2093.

(44) We include the interaction between two molecules if the closest distance between their atoms is smaller than a cutoff distance of 5.5 Å.

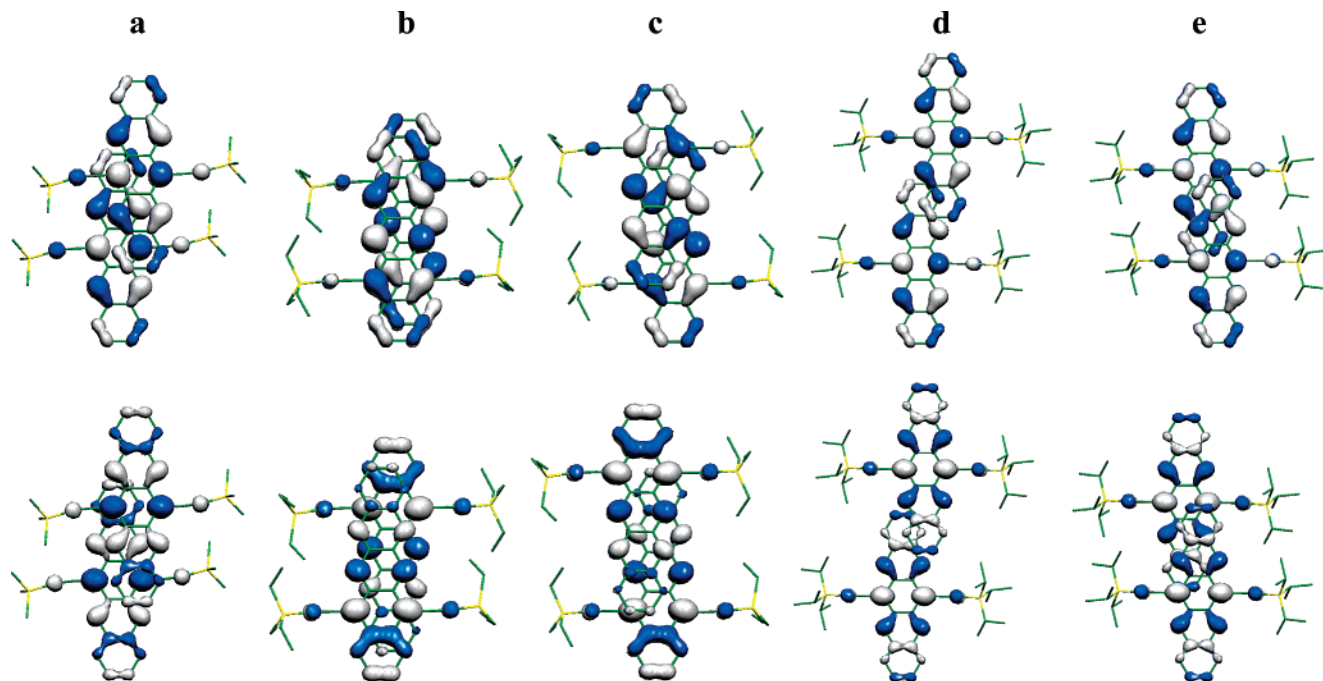


Figure 2. Plot of the two HOMOs (above) and the two LUMOs (below) of the five couples of close molecules with the strongest electronic interaction between the localized frontier MOs. The labels **a–e** correspond to that indicated in Table 1.

We note that these systems are very large compared to the one for which solid-state computational packages are optimized. For example, TESO contains eight molecules in the unit cell, which bring to ~ 5500 the number of basis functions required to perform a calculation with a 6-31G* basis set. The tight binding approach based on a subset of localized MO seems to be a viable approach to perform computations for which smaller and larger systems are treated with an identical and sufficiently good level of approximation.²⁸ Moreover, as we will see in section 3, the insight provided by a description based on the MOs can be extremely valuable.

Results. A selection of the matrix elements $V_{\alpha\beta T}$, required to compute the band structure of the three materials, is collected in Table 1. We reported the coupling between HOMO orbitals and between LUMO orbitals for all the couples of molecules considered in the calculation of TMS and TIPS (that have one molecule per unit cell). For the TESO solid (which has eight molecules per cell) we reported only the couples formed by one selected molecule with all the neighbors with non-negligible coupling. The pattern of the couplings with the neighbors is similar for all the other molecules in the unit cell.

Table 1 is a useful tool to link the band structure with chemical intuition. Each entry of the table can be visualized as a couple of molecules dressed with the corresponding MO and, from these drawings, it can be verified how a larger coupling is associated with a larger overlap between the MOs. We labeled as **a**, **b**, **c**, **d**, and **e** the five entries of Table 1 that correspond to couples in which the pentacene fragments are in face-to-face contact. This class of solids was designed to maximize the interaction between the couples labeled as **a–e**, and according to the predictions, these couples show the largest HOMO–HOMO and LUMO–LUMO coupling. We represented the interacting orbitals for

these five cases in Figure 2. While it seems obvious why the frontier orbital of the couples **a–e** are more strongly coupled than the others, it is not immediately clear what determines the difference in magnitude and sign among their coupling. In the next section we try to rationalize these differences by providing some general directions for the maximization of the coupling.

We conclude this section by presenting the computed bands for the three solids (Figure 3). The band dispersion is negligible in the directions along which the molecules are in contact through their alkylic portions (\vec{b} and \vec{c} , for TMS, \vec{a} and \vec{c} for TESO, and \vec{c} for TIPS). From the computed band structure we expect an essentially one-dimensional conduction along the crystal \vec{a} and \vec{c} axis for TMS and TESO, respectively, and a two-dimensional conduction in the ab plane for the TIPS-based material. We note that in molecular crystals there is a very good correlation between bands and MOs of the isolated molecule, because the bands originating from different MOs do not mix. For this reason it is very often found that the information contained in tables such as Table 1 is completely equivalent to the calculation of the band dispersion. We also note that the band structures for TMS and TIPS closely resemble those previously reported by Haddon et al.⁴⁵ using (single- ζ) extended Huckel calculations.

It should be remarked that the bandlike mechanism could be considered valid for organic semiconductors only at very low temperature. As noticed by several authors,^{23,46} the mean free path of the charge carrier drops to values on the order of magnitude of the crystal unit cell at temperatures above

(45) Haddon, R. C.; Chi, X.; Itkis, M. E.; Anthony, J. E.; Eaton, D. L.; Siegrist, T.; Mattheus, C. C.; Palstra, T. T. M. *J. Phys. Chem. B* **2002**, *106*, 8288.

(46) Kenkre, V. M.; Andersen, J. D.; Dunlap, D. H.; Duke, C. B. *Phys. Rev. Lett.* **1989**, *62*, 1165.

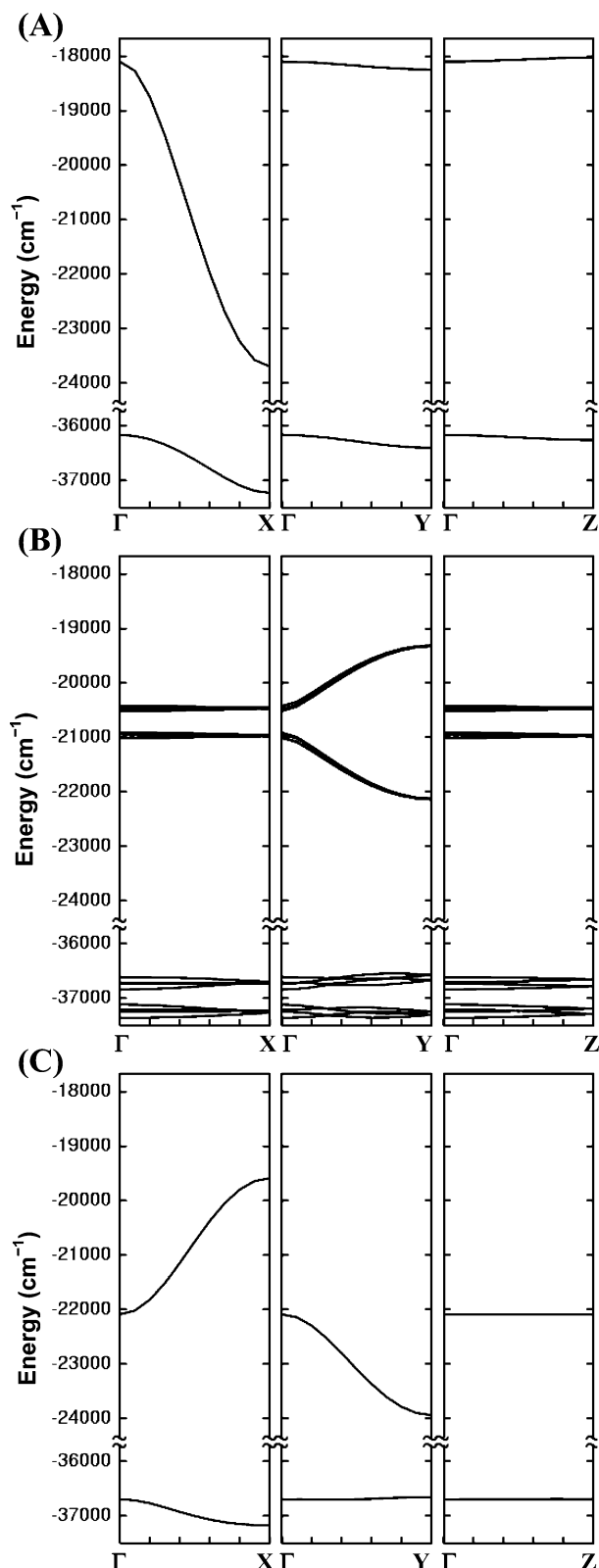


Figure 3. Band structure of (A) TMS, (B) TESO, and (C) TIPS. The labeled points indicate the following positions (in terms of reciprocal space unit vectors), Γ (0, 0, 0), X ($1/2$, 0, 0), Y (0, $1/2$, 0), Z (0, 0, $1/2$). One occupied and one unoccupied band are shown in parts A and C (one molecule per unit cell). Eight occupied and eight unoccupied bands are shown in part B (eight molecules per unit cell); note the quartet of quasidegenerate bands.

~ 150 K, a fact that seems to contradict a delocalized picture. Experimentally, bandlike transport was found in a recent paper for pentacene and the materials studied in this paper up to room temperature,⁴⁷ in agreement with other similar

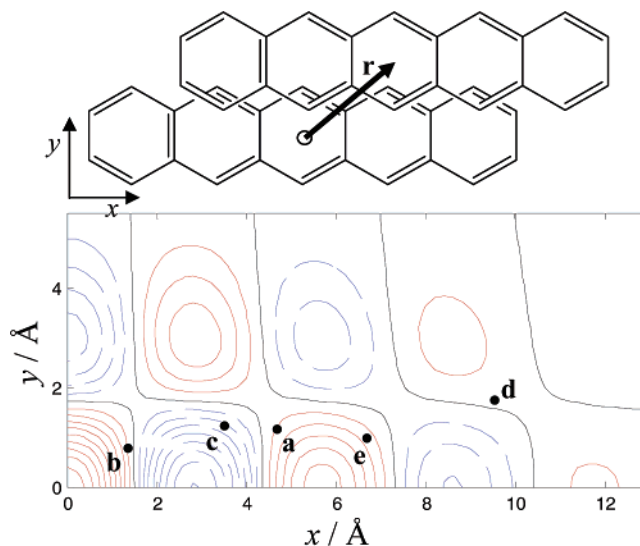


Figure 4. Map representing the electronic coupling between the HOMOs of two pentacene molecules laying on two parallel planes 3.4 \AA apart with an offset between their centers of mass given by x and y (x, y are the projections of the displacement \mathbf{r} on the longer and shorter pentacene symmetry axis in the plane of the molecule). Contour lines are plotted at intervals of 700 cm^{-1} ; the black contour line corresponds to the null coupling (nodal plane); dashed blue and solid red lines indicate negative and positive values. The labels a–e indicate the actual position of the pentacene fragments present in the material studied in this paper (see Table 1).

observations for pure pentacene thin films.⁴⁸ The complete clarification of the transport mechanism would probably require a detailed inclusion of all the effects deriving from the coupling between electronic and nuclear degree of freedom. One aspect of this coupling will be discussed in section 4 of this paper.

3. Rationalization

The inspection of Figure 1 does not suggest any simple reason to explain the trend in the coupling magnitude computed for the corresponding entries in Table 1. If the coupling depended on the finer detail of the calculation without any possible rationalization, the design of new and better organic semiconductors would not be possible. We will explore in this section the origin of the apparently chaotic behavior of the coupling magnitude showing, indeed, that it is possible to define few rules for the design of new materials of this class with improved intermolecular coupling.

Map of the Coupling. We focus on the coupling between HOMO orbitals in pentacene derivatives, stating similarities and differences for the LUMOs' case at the end of this section. The HOMO of the pentacene derivatives considered in this paper correlates very well with the HOMO of the pentacene without substituents.⁴⁹ We computed the map of the coupling between two pentacene molecules sliding one with respect to the other on two parallel planes distant 3.4 \AA , as illustrated in Figure 4 (their relative orientation is kept fixed). The x and y parameters describe the shift of one of the molecules in the direction of its longer or shorter axis,

(47) Ostroverkhova, O.; Cooke, D. G.; Shcherbyna, S.; Egerton, R. F.; Hegmann, F. A.; Tykwinski, R. R.; Anthony, J. E. *Phys. Rev. B* **2005**, *71*, 035204.

(48) Jurchescu, O. D.; Baas, J.; Palstra, T. T. M. *Appl. Phys. Lett.* **2004**, *84*, 3061.

being the (0,0) position correspondent to the mirror symmetric perfect pairing. A similar map was built by Kazmaier and Hoffmann to analyze the optical absorption of several perylene derivatives.⁵⁰

The map of the HOMO–HOMO coupling $V_{\text{HH}}(x,y)$, for $x,y > 0$, is reported in Figure 4. The maximum coupling ($\sim 6000 \text{ cm}^{-1}$) is found at the (0,0) position, where the overlap between the two orbitals reaches its most negative value. The (positive) maxima or (negative) minima of the coupling follow the minima and maxima of the interorbital overlap, and the absolute value of the coupling in these maxima or minima becomes smaller as the distance between the center of mass of the pentacene molecules increases. The coupling map shows nodal planes that correspond to the nodal planes of the interacting orbitals. We note, in particular, that the HOMO orbital of pentacene (which, as for other oligoacenes, transforms as the b_{3g} representation of the D_{2h} point group) has a nodal plane coincident with its σ_{xz} symmetry plane that shows up in the coupling map as a node parallel to the x axis with $y = 1.72 \text{ \AA}$.

Position of Real Systems in the Map and Consequences.

We can find on the above-described map the position of the five distinct couples of cofacial pentacene fragments found in the three considered materials (entries **a–e** of Table 1 and Figure 2).⁵¹ We found that that all five couples are in a mutual position that corresponds to a point close to the nodal plane of the V_{HH} coupling map. In particular, all experimental pairs of coplanar pentacene fragments show an offset along the y direction between 0.8 and 1.8 \AA , therefore close to the nodal plane with $y = 1.72 \text{ \AA}$.

The reason for this positioning is easily understandable in terms of rigid sphere packing. If we model the pentacene as a collection of 22 rigid spheres centered on the carbon atoms, the best coplanar packing requires an offset of the atom layers (the face to face packing of two pentacene molecules can be considered akin to that of two adjacent planes of graphite). Because of the Coulomb and Pauli repulsion between the electronic clouds surrounding the carbon atoms, the energetically most favorable packing brings the molecules to a more unfavorable position for the electronic coupling.

Near the nodal plane, the sign and magnitude of the coupling are extremely dependent on the precise position of the two molecules, and for this reason it is very difficult to predict the coupling magnitude from the inspection of Figure 2 or similar plots. However, the coupling map of Figure 4 (which does not consider the effect of the pentacene substituents), provides a useful guide for the rationalization of the five couplings **a–e**. For example, we can note that there is a precise match between the sign of the computed coupling and the corresponding sign in the coupling map

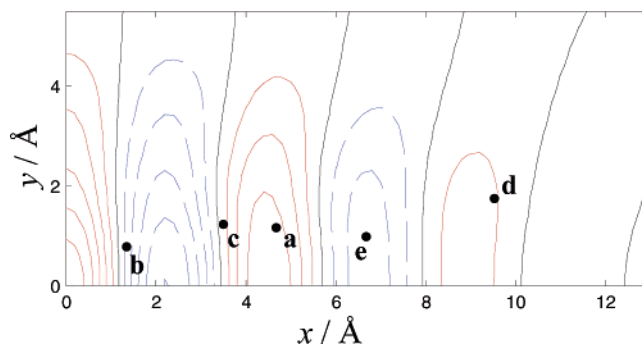


Figure 5. Map representing the electronic coupling between the LUMOs of two pentacene molecules. See the description in Figure 4. Contour lines are plotted at intervals of 700 cm^{-1} .

for the unsubstituted pentacene. Moreover, the largest coupling V_{HH} in absolute value (**c**) corresponds to the point further away from the nodal planes, while the coupling between the molecules of the couple **e** is the smallest, because the distance between the two centers of mass is too large.

The map also can be helpful in suggesting strategies to maximize the coupling between HOMOs for the design of better p-type semiconductors based on this class of molecules. A moderate increase of the coupling can be achieved by reducing the offset of the molecules along the x axis, while a great increase of the coupling could be achieved by reducing the offset along the y axis below the current limit of 0.8 \AA . The bulky pentacene substituents have been used to force the pentacene fragments in a coplanar packing instead of the herringbone arrangement typical of unsubstituted polyacenes. It is probably possible to design an appropriate substitution of the pentacene moiety whose interaction with the neighbors is strong enough to force a pair of pentacene fragments in the higher coupling configurations with a reduced offset along the y direction. The map of the LUMO–LUMO coupling $V_{\text{LL}}(x,y)$ is shown in Figure 5. As for the other oligoacenes, the LUMO transform as the b_{1u} representation and it has no nodal plane corresponding to its σ_{xz} symmetry plane. Consequently, in the coupling map we do not find the nodal plane parallel to the x axis but a larger number of nodal planes parallel to y axis. The absence of the nodal plane at $y = 1.72 \text{ \AA}$, close to the actual position of the **a–e** couple, is one of the reasons for the higher values of coupling between these LUMO orbitals in Table 1 (the other reason is that the LUMO orbitals are slightly more extended along the z direction). As in the previous case, there is a good correspondence in sign and magnitude between the position in the map of the **a–e** couples and the accurate calculations of Table 1. In contrast to the HOMO case, there are two molecule pairs, **a** and **e**, that are far from all nodal planes of the coupling map and are consequently associated with the highest values of the LUMO–LUMO coupling. The comparison of Figure 4 with Figure 5 suggests that it is easier to get greater absolute coupling between LUMOs using face-to-face pentacene units and that packing motifs similar to that of TMS and TIPS may be useful for the construction of n-type semiconductors.⁵ Research on n-type materials is focusing on compounds that can be easily reduced in solution,^{16,52} but also a large LUMO–LUMO coupling is desirable because it increases the electron mobility and

(49) Although the HOMO shape is marginally affected by the functionalization, the oxidation potential of these substituted pentacenes is $\sim 66\,000 \text{ cm}^{-1}$ higher than that of unsubstituted pentacene.

(50) Kazmaier, P. M.; Hoffmann, R. *J. Am. Chem. Soc.* **1994**, *116*, 9684.

(51) The idealized planar pentacene geometry overlapped the pentacene fragments in the experimental structure. For each cofacial pair, the center of mass of one molecule was projected on the plane defined by the other molecule to get the (x,y) coordinate represented in Figure 2.

decreases the reduction potential in the solid (facilitating the charge injection).

4. Effect of Thermal Motions of the Intermolecular Coupling

The considerations of the previous section assumed a static view of the crystal, a view that is justified at low-temperature assuming a negligible electron–phonon coupling. However, these large molecules have several low-frequency vibrational modes that can be populated at room temperature and that can influence the intermolecular coupling.

Consequences on the Transport Properties. The pentacene fragments, for all the face-to-face couples of these materials, are in the relative position where the coupling between HOMOs is the most sensitive to the geometric parameters. In other words, since the molecule pair is positioned close to the nodal plane of the HOMO coupling map, any small displacement causes a large change in the coupling. It is therefore natural to expect that the thermal motions enhance the intermolecular interaction, introducing at the same time disorder and loss of coherence in the electron motion.

We will describe, only for TMS, the effect of the thermal motions on the most important intermolecular coupling, and we will report the average and the variance of the coupling at different temperatures. TMS solid was chosen for simplicity, because it forms a one-dimensional stack along the \vec{a} axis of the crystal with only one molecule pair with a substantial coupling between HOMOs and LUMOs (i.e. entry **a** of Table 1).

Molecular Dynamics Simulation. We replicated the unit cell of TMS generating the $4 \times 3 \times 3$ supercell used in the molecular dynamics (MD) simulation (in this way each molecule is not in contact with its image). We used the MM3 force field⁵³ to simulate the classical motions of the nuclei. This force field was parametrized to reproduce the packing of organic molecular crystal, and its use seems particularly suited to this problem. MD calculations were run at constant temperature within the canonical ensemble using the Berendsen⁵⁴ algorithm. Hydrogen atoms were constrained at their ideal bond distance using the RATTLE algorithm,⁵⁵ while the remaining degrees of freedom were left flexible. The integration time step was 2 fs. We run simulations at 100 and 300 K, analyzing the results after 10 ps of equilibration.

Every $\delta t = 0.1$ ps we computed the electronic coupling, V_{HH} and V_{LL} , between the adjacent molecules in the supercell, as described in section 1. The adjacent molecules correspond to the couple **a** of Table 1. This was the most computationally demanding part of the procedure that limited the time of the analyzed trajectory to 50 ps. To speed up the calculation, we reduced the computational level for the calculation of the orbitals and their coupling to HF/3-21G.

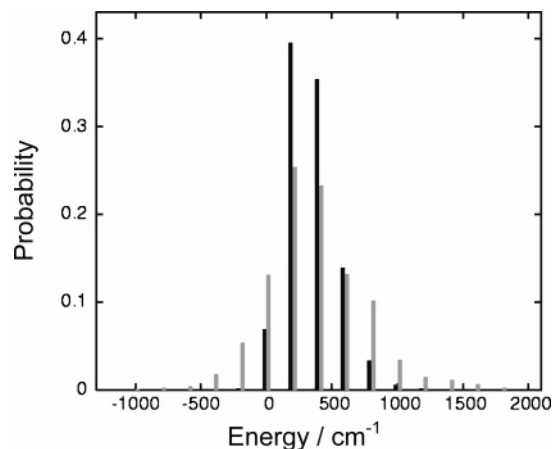


Figure 6. Distribution function of the V_{HH} coupling between adjacent molecules of a $4 \times 3 \times 3$ supercell of TMS (coupling **a** of Table 1). Black and gray histograms refer to the simulation at 100 and 300 K, respectively.

Since the MOs are recomputed every snapshot, their sign, not maintained from one snapshot to the other, is arbitrary, as well as the sign of the interorbital coupling. To avoid this problem (which prevents the proper calculation of the coupling distribution function) we compared at each time $t = t_1$ the sign of the orbital with the sign of the same orbital in the previous snapshot $t = t_1 - \delta t$, and if the sign is changed, we multiply the orbital by -1 .

Analysis. The distribution of V_{HH} at the two temperatures is shown in Figure 6. The distribution is approximately Gaussian, with the average value and standard deviation given by 340 ± 186 and 366 ± 371 cm^{-1} , respectively, at 100 and 300 K. The distribution of V_{LL} is similar, with $V_{LL} = 1689 \pm 170$ cm^{-1} at 100 K and $V_{LL} = 1608 \pm 338$ cm^{-1} at 300 K. Clearly, the most important outcome of this calculation is the huge variance of the coupling already at relatively low temperature. The role of thermal motions is probably more important for the V_{HH} coupling, which has a variance of the same magnitude of the average coupling. The larger relative fluctuations of the HOMO coupling can be understood by comparing the position of the pentacene couple **a** in Figures 4 and 5: **a**, being closer to a nodal plane of $V_{HH}(x,y)$, the V_{HH} coupling is more sensitive to small changes in the geometry than V_{LL} . We note also that the large variance of the intermolecular coupling is due to the weak interaction among individual molecules described by the nonbonded (van der Waals) terms of the force field. Since these terms are similar among different force fields, the choice of the force field does not affect the main conclusions of this section.

To visualize the conformational space visited by the MD simulation, we showed in Figure 7 the overlapped structures of 50 snapshots of the simulation. To better understand the effect of this motion on the coupling, we plotted (Figure 7) on the HOMO coupling map the relative position of the pentacene fragments in 400 snapshots of the simulation as done for the five molecule pairs in Figures 4 and 5. Obviously, while the map was build using rigid molecules that kept their relative orientation, the thermal motions also cause slight deformation of the molecules and change in their relative orientation. Figures 6 and 7 illustrate that, even in the crystal phase, the limited conformational space explored

(52) Chesterfield, R. J.; Newman, C. R.; Pappenfus, T. M.; Ewbank, P. C.; Haukaas, M. H.; Mann, K. R.; Miller, L. L.; Frisbie, C. D. *Adv. Mater.* **2003**, *15*, 1278.

(53) Allinger, N. L.; Li, F.; Yan, L.; Tai, J. C. *J. Comput. Chem.* **1990**, *11*, 868.

(54) Berendsen, H. J. C.; Postma, J. P. M.; van Gunsteren, W. F.; di Nola, A.; Haak, J. R. *J. Chem. Phys.* **1984**, *81*, 3684.

(55) Andersen, H. C. *J. Comput. Phys.* **1983**, *52*, 24.

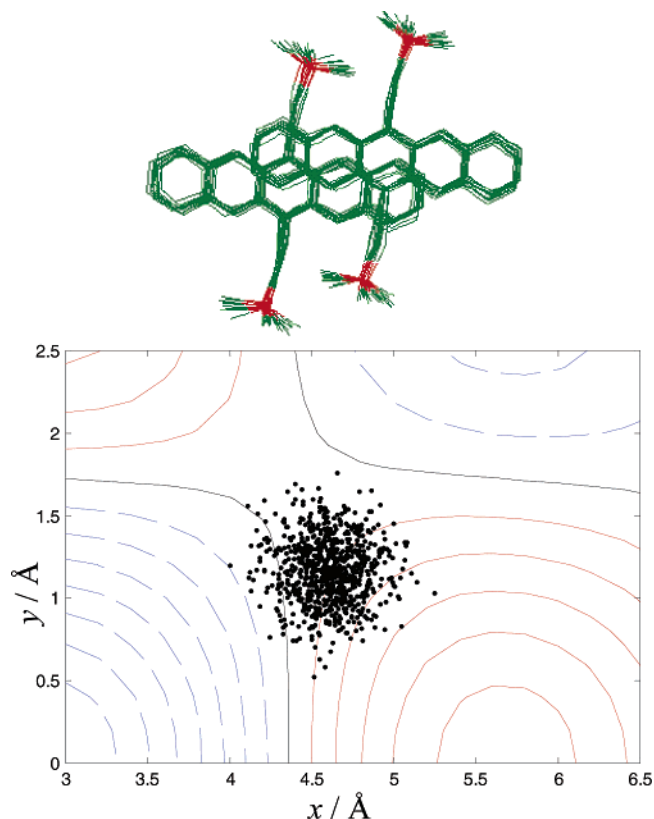


Figure 7. (Top) Overlapped geometries of a couple of TMS molecules derived from 50 snapshots of a MD simulation. (Bottom) The black dots represent the relative position of the pentacene fragment during the dynamics (taken every 0.1 ps) in terms of their relative offset, as described in Figure 4. The contour lines reproduce the V_{HH} coupling map of Figure 4.

at room temperature is large enough to produce consistent variation in the intermolecular coupling.

The effect of the thermal disorder on the electronic structure of these materials can be dramatic. The fluctuation of the intermolecular coupling causes localization^{56,57} of the wave function and frequent loss of coherence of the electronic motion. We argue that this dynamic disorder is related to the very small mean free path of the charge carrier that these materials appear to have,²³ and a detailed theoretical modeling of the electron dynamics will be presented elsewhere. A practical aspect of the role of disorder is the sensitivity of these materials to thermal energy, as reported in refs 7 and 58. From a “use” perspective, a relatively poor electronic conductor with strong electron–phonon coupling may lead to new thermal management materials for use in the semiconductor industry or biosensing.⁵⁹

Since the charge localization induced by the thermal disorder can be the limiting factor for the measured mobility, the attempt to rationalize experimental results through the

comparison of intermolecular coupling strength should be complemented by an estimate of the importance of thermal motion on the relevant coupling. According to this view, molecular pairs whose coupling is close to a nodal plane of the coupling map are less efficient in mediating the charge transport. For example, the persistent photocurrent measured for TIPS⁶⁰ is not only related to the high coupling between its LUMOs but it is probably also due to the position of the couple e in the LUMO’s coupling map (Figure 5). In fact, the LUMO coupling e is not only high but also less sensitive than in other compounds to thermal motions, because it is further away from the node in the coupling map.

5. Conclusion

We computed the intermolecular electronic coupling and the band structure of three pentacene derivatives, discussing their possible application in organic electronics. To better rationalize the results found for the three crystals, we built a map of the coupling between a pair of coplanar unsubstituted pentacene molecules, and we found that the actual interacting pair of pentacene derivatives are often found in the region of the map closer to a nodal plane, where the sensitivity to the smallest structural deformation is higher. We noted how the coupling map between HOMOs and LUMOs of the unsubstituted pentacene can be used as a guide for the design of material with stronger interaction.

From the coupling map it could be inferred that thermal motions could substantially modulate the intermolecular coupling. We investigate in detail this aspect for the TMS-based material, running a molecular dynamics simulation and computing the intermolecular coupling for several hundreds of snapshots. We have found that the off-diagonal disorder (fluctuation of the intermolecular coupling) is very large for this class of systems, and it certainly plays an important role in the transport mechanism. The difficulties in relating intuitively the crystal structure of a material with its electric transport properties are probably also related to the huge effect of thermal motions, which cannot be considered a small perturbation over the ideally frozen crystal structure. The computational findings of this paper also suggest that the usual perturbative treatment of the electron–phonon coupling can be inadequate for organic semiconductors, for which this coupling is large and affects the zeroth order description. A mathematical framework suitable for the modeling of the transport under these conditions is currently under development.

Acknowledgment. A.T. and G.O. gratefully thank MIUR for support (projects “Dinamiche Molecolari in Sistemi di Interesse Chimico” and “Microstrutture e nano-strutture a base di carbonio”). J.E.A. wishes to thank the Office of Naval Research for support of his research on pentacene.

CM051150H

(56) Anderson, P. W. *Phys. Rev.* **1958**, *109*, 1492.
 (57) Lee, P. A.; Ramakrishnan, T. V. *Rev. Mod. Phys.* **1985**, *57*, 287.
 (58) Tokumoto, T.; Brooks, J. S.; Clinite, R.; Wei, X.; Anthony, J. E.; Eaton, D. L.; Parkin, S. R. *J. Appl. Phys.* **2002**, *92*, 5208.
 (59) Someya, T.; Sekitani, T.; Iba, S.; Kato, Y.; Kawaguchi, H.; Sakurai, T. *Proc. Natl. Acad. Sci. U.S.A.* **2004**, *101*, 9966.

(60) Brooks, J. S.; Tokumoto, T.; Choi, E. S.; Graf, D.; Biskup, N.; Eaton, D. L.; Anthony, J. E.; Odom, S. A. *J. Appl. Phys.* **2004**, *96*, 3312.